Journal of Magnetism and Magnetic Materials 343 (2013) 169–172

Contents lists available at SciVerse ScienceDirect

Journal of Magnetism and Magnetic Materials

journal homepage: www.elsevier.com/locate/jmmm

Modification in martensite morphology and magneto-strain through rapid solidification and heat treatment of NiMnGaAl alloy

Satnam Singh [a], R.K. Roy [a], M. Ghosh [a], N.B. Manik [b], A. Mitra [a], A.K. Panda [a,*]

[a] CSIR-National Metallurgical Laboratory, Jamshedpur, India
[b] Jadavpur University, Kolkata, India

ARTICLE INFO

Article history:
Received 25 January 2013
Received in revised form
3 May 2013
Available online 14 May 2013

Keywords:
Rapid quenching
Melt spinning
Magnetic field induced strain
Martensite
Austenite

ABSTRACT

The influence of melt spinning and heat treatment on the structure, phase transformation and magnetic field induced strain (MFIS) properties have been investigated for $Ni_{55}Mn_{22}Ga_{22}Al_1$ (at%) alloy. The microstructure showed distinct improvement in morphology of as spun ribbon as compared to ingot. Annealing further enhanced martensite state and displayed systematic arrangement of dislocations. It contributed to increase MFIS to 482 ppm in annealed ribbon as compared to 190 ppm and 28 ppm for as-spun ribbon and ingot, respectively.

1. Introduction

The research on the NiMnGa Ferromagnetic Shape Memory Alloys (FSMAs) since past few years is focused on understanding the influence of thermo-kinetics on the structural, magnetic and transformation properties of the alloy [1–3]. The parameters like quenching temperature, cooling rate and annealing have strong influence on magnetic shape memory behavior of the alloy [1,3]. The quenching temperature affects the atomic ordering and stability of phases at room temperature [1]. The ordering will be high if the alloy is quenched from its ordering temperature ($L2_1 \leftrightarrow B2$) [2] and less when quenched from a temperature higher than ordering temperature [1–3]. Thus structural and magnetic transformations are influenced by quenching conditions [3]. High cooling rate not only reduces grain size [4], generates new phases [6] but also modifies crystal periodicity [7]. Recent investigations on rapid quenching from the liquid state using melt spinning technique reveal interesting properties of Ferromagnetic Shape Memory Alloys (FSMAs) [5–13]. The ribbons prepared by melt spinning technique exhibit reduced martensite transformation temperature as well as enthalpy of transformation [5]. Both these thermodynamic parameters which depend on wheel speed (quenching rate) of the melt spinning technique reduce with the increase in wheel speed [8]. The reported Curie temperature is also less in as-spun ribbons as compared to the bulk alloys of similar composition [9,10]. These effects can be correlated to the quenched-in structure of the ribbons [4,10,11]. The ribbons are polycrystalline alloys of small grained cellular structures with dendrite morphology [5,12]. The rapid quenching through melt spinning has been reported to change layer periodicity in ribbons from a non-modulated structure to 7 M and/or 10 M layered one [7]. As-spun ribbons have also found to exhibit textured microstructure with large magneto-crystalline anisotropy favoring magnetic field induced strain (MFIS) [5,13]. The present investigations is an attempt to address the effects of melt spinning and annealing on the structural, magnetic, thermal and MFIS behavior of a $Ni_{55}Mn_{22}Ga_{22}Al_1$(at%) ferromagnetic shape memory alloy.

2. Experimental

Pure elements with purity greater than 99.5% has been used for preparing $Ni_{55}Mn_{22}Ga_{22}Al_1$ (at%) alloy. An ingot of the alloy was prepared using argon arc melting followed by induction melting in argon atmosphere for ensuring compositional homogeneity. The ingot was induction melted and as-spun to ribbons. To enhance ordering the as-spun ribbon and ingot were annealed in argon ambient at 800 °C for 30 h. The samples of annealed ingot, as-spun ribbon and annealed ribbon are designated as S_I, S_R, S_{RAN} respectively. All these samples were simultaneously characterized for comparing their properties. The Bruker AXS D8 x-ray diffractometer with Cu-Kα target was used for structural investigations. Transmission Electron Microscopy (Philips CM200: TEM) was

* Corresponding author. Tel.: +91 657 2345002; fax: +91 657 2345213.
E-mail addresses: akpanda2_in@rediffmail.com, akpanda@nmlindia.org (A.K. Panda).

0304-8853/$ - see front matter © 2013 Published by Elsevier B.V.
http://dx.doi.org/10.1016/j.jmmm.2013.05.005

carried out for understanding microscopic features. The thermal kinetics and martensite transformation temperatures were observed using Differential scanning calorimeter (Pyris: Diamond DSC) at a scan rate of 15 K/min. Thermo-magnetic measurements and room temperature magnetization were carried out using vibrating sample magnetometer (LakeShore VSM-7404) at a temperature scan rate of 2 K/min. The MFIS measurement was carried out using a device based on two terminal capacitor system developed in laboratory.

3. Results and discussion

The x-ray diffraction studies carried out at room temperature (Fig. 1) showed existence of martensite phase in ingot and annealed ribbon. However the as-spun ribbon revealed an additional austenite phase along with martensite phase. Reference peak reflections support martensite to have I4/mmm space group symmetric tetragonal phase. The lattice parameters for the martensite phase calculated from the peaks are shown in Table 1. The tetragonality ratio 'c/a' for the martensite phase is lower in case of as-spun ribbon as compared to ingot. On annealing the c/a ratio of annealed ribbons become greater than that of the ingot. However the high cell volume of ribbon reduced on annealing and was lower than that of the ingot. The additional austenite phase in as-spun ribbons is cubic with lattice constant $a=5.758$ Å and the space group symmetry Fm3m. The presence of this phase has been observed in our earlier investigations [6]. It is suggested that the austenite phase is the influence of rapid quenching. Kressel et al. have predicted about its presence in the alloys rapidly quenching from the B2 domain of T–C diagram [3]. However, this phase could not be observed in some reports [1,3,15]. It may be due to insufficient quenching rate during their experiments. In the present case the process of melt spinning with high quenching rate of

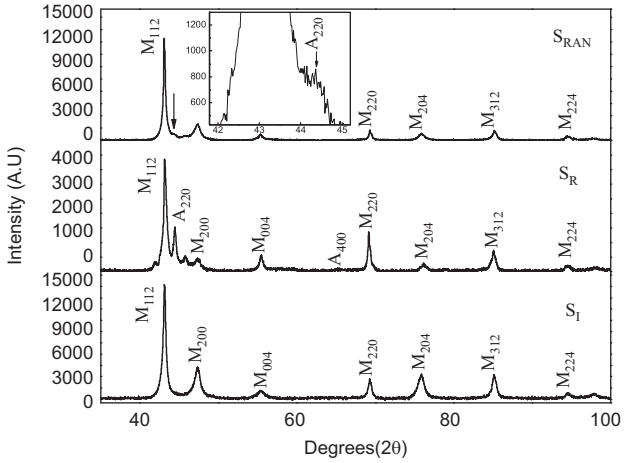

Fig. 1. The x-ray diffractograms indicating martensite phase (M) in ingot and annealed ribbon and a combination of martensite (M) and austenite (A) phases in as-spun ribbon. A small A_{220} peak (inset) is an indication of retained austenite phase in annealed ribbon.

Table 1
The lattice parameter, cell volume and lattice strain of ingot, as-spun ribbon and annealed ribbon.

Sample	'a' (Å)	'c' (Å)	c/a	Cell volume (Å^3)	Lattice strain (ppm)
S_I	3.834	6.611	1.724	97.18	5500
S_R	3.837	6.606	1.721	97.32	3800
S_{RAN}	3.827	6.617	1.729	96.945	3600

10^{-5} K/s as compared to water quenching (10^{-2} K/s) leads to frozen in austenite phase. Annealing the ribbons at 800 °C for 30 h has reduced the austenite phase. Only a small fraction of austenite phase is displayed by small (A_{220}) peak (inset, Fig. 1). Peak broadening analysis through 'Strokes and Wilson formula' carried out to understand effect of high cooling rate on the lattice strain is given in Table 1. The results reveal largest lattice strain of 5500 ppm in ingot, whereas the strain is smaller in as spun ribbon and annealed ribbon. Usually rapid quenching increases strain in the material [3]. However the reverse effects are expected to occur because of micro-structural changes during melt spinning.

The difference in quenching rates of air cooled ingot and as-spun ribbon as well as annealed ribbon exhibited interesting effects on the microstructures (Fig. 2). Although both the ingot and as-spun ribbon exhibited twinned microstructure, as-spun ribbons revealed more systematic arrangement of twins. In the case of ingot the twins are oriented in different directions intersecting each other (Fig. 2a). This morphology showed not only high dislocation density but also closed proximal variants. A selected martensite phase with single untwined zone is shown in Fig. 2b. This untwined region is revealed in the SAD pattern (inset, Fig. 2b). The large lattice strain (5400 ppm) obtained from x-ray peak broadening analysis is expected to be originated from randomly arranged high dislocation density in ingot (Table 1). In contrast to the ingot, martensite twins within as-spun ribbons display extended morphology and dislocations are more systematically arranged (Fig. 2c). As a result the lattice strain in as-spun ribbon showed small value of 3800 ppm. Annealing the ribbons at 800 °C for 30 h further enhanced the micro-structure. The martensite twins of annealed ribbons become broader and extended (Fig. 2d) and dislocations piled up closed to the grain boundaries or arranged much more systematically. Annealing also reduced the residual strain produced during rapid quenching of ribbon, therefore reducing the calculated lattice strain in annealed ribbons to an even lower value of 3600 ppm as compared to the as-spun ribbon.

The Differential Scanning Calorimeter revealed the interesting thermo-kinetic and transformation distinctions between ingot, as-spun ribbon and annealed ribbons (Fig. 3). The transformation in as spun ribbons is distinctly a single step transformation as compared to multi-steps indicated in transformation profiles of ingot. The martensite transformation temperature (M_S), its reverse (A_S) and transformation enthalpies of the as-spun ribbons are lower than those of ingot (Table 2). The existence of parent austenite phase in as-spun ribbon along with martensite is supposed to lower its transformation temperature (M_S, A_S). It also lowers the span of transformation ($\Delta M=M_S-M_S$) and its reverse ($\Delta A=A_F-A_S$) in as-spun ribbon compared to ingot (Table 2). On the other hand, ingot with predominantly martensite phase revealed much lesser span of transformation. Interestingly the annealed ribbon exhibited transformation span in between as-spun ribbon and ingot because of very small fraction of austenite phase. The austenite phase existing at room temperature does not undergo martensite transformation; thus the transformation enthalpy of as-spun ribbons is lower than that of ingot. In annealed ribbons this phase is nearly absent (inset, Fig. 1); therefore the observed transformation enthalpy is higher than as-spun ribbons but less than fully martensitic ingot.

Thermal and structural properties of the alloy correlatively influenced the magnetic behavior. The thermo-magnetic $M[T]$ investigations (Fig. 4) revealed lower magnetic ordering temperature (T_C) of 348 K in as-spun ribbons as compared to 363 K in the ingot. The presence of low fraction of austenite having reduced ferromagnetic ordering temperature lowered the TC of as-spun ribbon compared to ingot [16]. In the annealed state as the volume fraction of austenite phase is reduced leading to elevation in the magnetic ordering temperature $T_C=354$ K. This observation is in

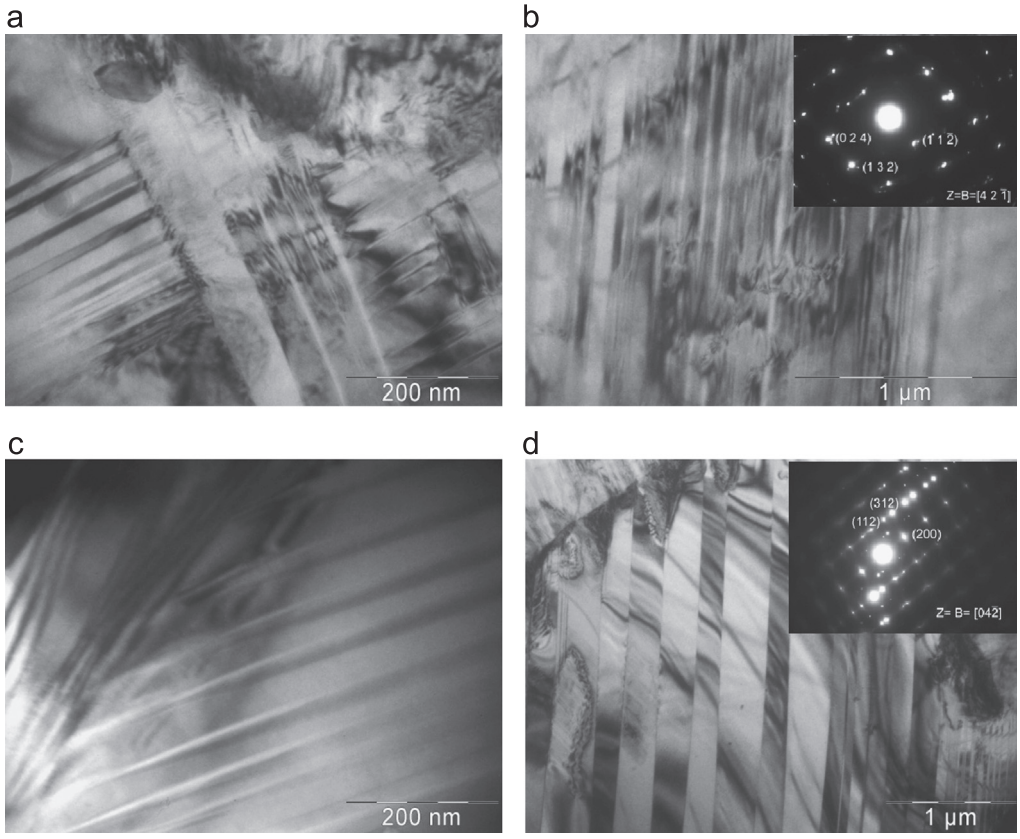

Fig. 2. The TEM images of (a) and (b) ingot (c) as-spun ribbon and (d) annealed ribbon. The SAD patterns are given in inset.

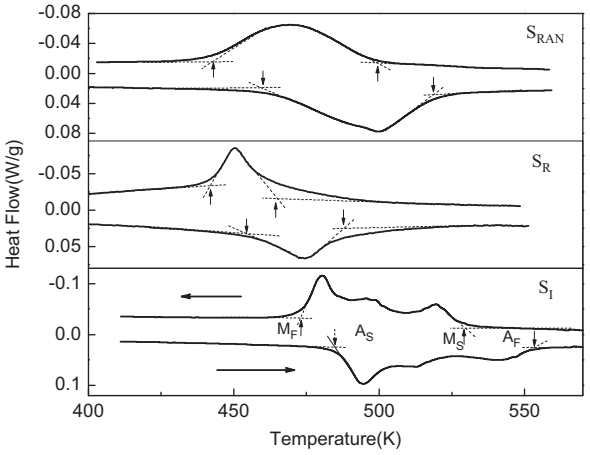

Fig. 3. The DSC studies revealed martensite transformation behavior for ingot, as-spun ribbon and annealed ribbon.

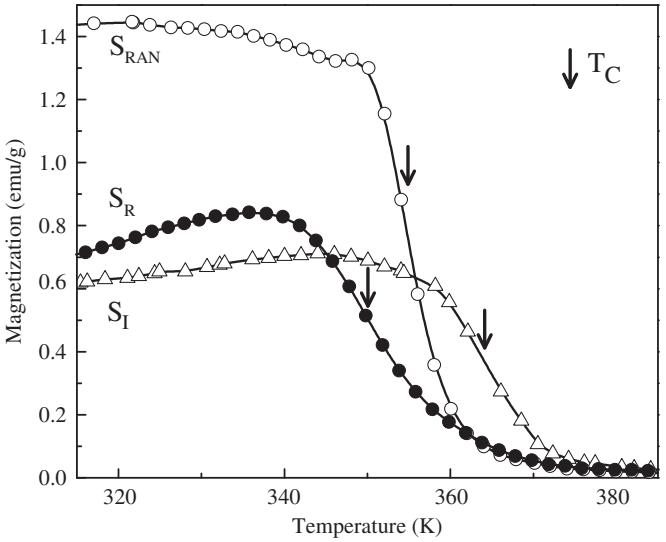

Fig. 4. The thermo-magnetic curves indicating magnetic ordering temperature for ingot, 363 K; as-spun ribbon, 349 K; and annealed ribbon, 354 K.

Table 2
The structural transformation temperatures and enthalpies of ingot, as-spun ribbon, and annealed ribbon.

Sample	A_S (K)	A_F (K)	$\Delta A = A_F - A_S$	M_S (K)	M_F (K)	$\Delta M = M_S - M_S$	$\Delta H(H)$ (J/g)	$\Delta H(C)$ (J/g)
S_I	484	553	69	530	471	59	8.6	7.4
S_R	457	491	34	468	443	35	5.1	4.3
S_{RAN}	460	517	57	499	441	58	7.7	6.7

agreement with the reported investigation [10,14]. The saturation magnetization value of as-spun ribbon and annealed ribbon is almost similar ~46 emu/g, indicating that small fraction of austenite with martensite does not manifest distinct magnetization levels. Interestingly, the saturation magnetization of ingot is lower with a value of 40 emu/g. Its high value of lattice strain ~5500 ppm and dislocation density in martensitic variants limit domain saturation [17]. From the magnetization plots, the coercivity (inset, Fig. 5) values of 5.8 mT and 4.4 mT for ingot and annealed ribbon respectively are lower compared to 14.7 mT obtained for as-spun ribbon. Martensite accommodation [11] and chemical ordering [13] during heat treatment is attributed to low coercivity values of annealed ingot and ribbon compared to

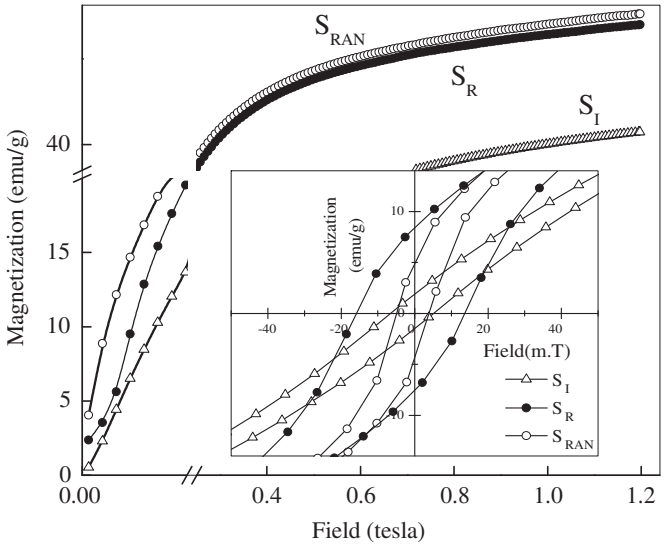

Fig. 5. The magnetization versus field curves indicating increased saturation magnetization in as-spun ribbons and further enhancement with annealing. The inset indicates respective variation in coercivity.

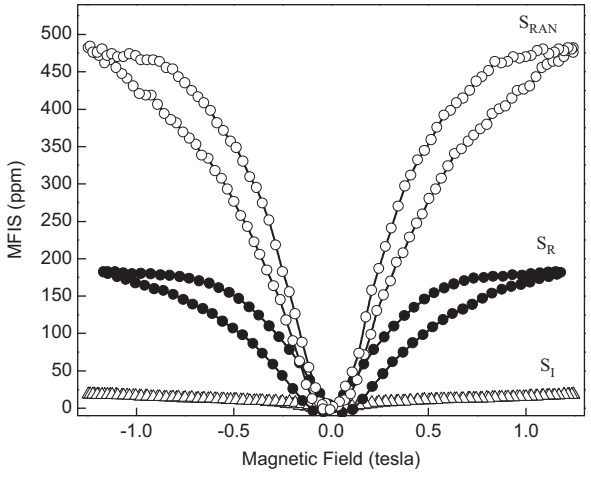

Fig. 6. The MFIS versus field curves for ingot, as-spun and annealed ribbon samples showing improvement in MFIS value after melt spinning and further enhancement with annealing.

as-spun ribbon. In contrast to annealed ribbon, the ingot even in its annealed state has high dislocation density which contributed to its magnetic hardening. This high density of dislocations acting as pinning centers toward domain wall propagation is responsible for higher coercivity of ingot.

The Magnetic field Induced strain (MFIS) for ingot, as-spun ribbon and annealed ribbon samples has been measured. The variation in the MFIS values with applied magnetizing field is shown in Fig. 6. A reversible MFIS of 28 ppm is observed in ingot at a magnetic field of 12 K G. It is far lower than a value of 190 ppm obtained for as spun ribbon. The effect has been correlated with a totally different microstructure of as-spun ribbons as compared to ingot (Fig. 2). The extended and wide martensite twins free from defects favor the magnetic field induced twin boundary motion (MFITBM) in as-spun ribbon. However in ingot the highly strained (5600 ppm) microstructure is responsible for its small MFIS of 28 ppm. The presence of small fraction of austenite in as-spun ribbon facilitated the field induced twinning and detwinning of martensite plates [18], resulting into its higher MFIS value than that of ingot. However, annealing provides highly ordered and accommodated martensite structure in terms of broader martensite twin plates along with systematic arrangement of dislocations (Fig. 2d). In this structure, the twin boundary movement is facilitated [19] and thus, led to a potential enhancement of MFIS from 190 ppm of as-spun ribbon to 482 ppm in annealed ribbon. The twinning–detwinning of martensite plates and existing internal fraction [20] showed some hysteresis in the as-spun and annealed ribbon compared to the ingot.

4. Conclusions

The rapid solidification through melt-spinning technique modified the phase transformation, structural and magnetic properties of $Ni_{55}Mn_{22}Ga_{22}Al_1$ (at%) alloy. The ribbon displayed martensite morphology with small fraction of the austenite phase. Annealing the ribbon improved martensite morphology with systematic arrangement of dislocations. As a result the annealed ribbon was magnetically softer than as-spun ribbon and ingot. All these factors contributed toward high MFIS in as spun ribbons as compared to ingot and toward further enhancement in annealed ribbons.

Acknowledgment

The financial assistance to one of the authors (Satnam Singh) by Council of Scientific and Industrial Research, India, is gratefully acknowledged.

References

[1] V. Sánchez-Alarcos, V. Recarte, J.I. Pérez-Landazábal, G.J. Cuello, Acta Materialia 55 (2007) 3883–3889.
[2] H. Ishikawa, R.Y. Umetsu, K. Kobayashi, A. Fujita, R. Kainuma, K. Ishida, Acta Materialia 56 (2008) 4789–4797.
[3] M. Kreissl, K.U. Neumann, T. Stephens, K.R.A. Ziebeck, Journal of Physics: Condensed Matter 15 (2003) 3831–3839.
[4] M. Kreissl, T. Kanomata, M. Matsumoto, K.U. Neumanna, B. Ouladdiaf, T. Stephens, K.R.A. Ziebeck, Journal of Magnetism and Magnetic Materials 272–276 (2004) 2033–2034.
[5] F. Albertini, S. Besseghini, A. Paoluzi, L. Pareti, M. Pasquale, F. Passaretti, C. P. Sasso, A. Stantero, E. Villa, Journal of Magnetism and Magnetic Materials 242–245 (2002) 1421–1424.
[6] A.K Panda, S. Singh, R.K. Roy, M Ghosh, A Mitra, Journal of Magnetism and Magnetic Materials 323 (2011) 1161–1169.
[7] J. Pons, C. Segui, V.A. Chernenko, E. Cesari, P. Ochin, R. Portier, Materials Science and Engineering A 273–275 (1999) 315–319.
[8] C.T Hu, T. Goryczka, D. Vokoun, Scripta Materialia 50 (2004) 539–542.
[9] R.K Singh, M. Shamsuddin, R. Gopalan, R.P. Mathur, V. Chandrasekaran, Materials Science and Engineering A 476 (2008) 195–200.
[10] J. Wang, C. Jiang, R. Techapiesancharoenkij, D. Bono, S.M. Allen, R.C. O'Handley, Journal of Applied Physics 106 (2009) 023923.
[11] S. Singh, R.K. Roy, M Ghosh, A Mitra, A.K Panda, Journal of Applied Physics 112 (2012) 103512.
[12] J Liu, J.G Li, Materials Science and Engineering A 454–455 (2007) 423–432.
[13] Z.H. Liu, J.L. Chen, H.N. Hu, M. Zhang, X.F. Dai, Z.Y. Zhu, G.D. Liu, G.H. Wu, F. B. Meng, Y.X. Li, Scripta Materialia 51 (2004) 1011–1015.
[14] V. Recarte, J.I. Pérez-Landazábal, C. Gomez-Polo, C. Seguí, E. Cesari, P. Ochin, Materials Science and Engineering A 438–440 (2006) 927–930.
[15] R.W Overholser, M. Wuttig, Scripta Materialia 40 (1999) 1095–1102.
[16] L Mañosa, A. Planes, M. Acet, E. Duman, E.F. Wassermann, Journal of Magnetism and Magnetic Materials 272–276 (2004) 2090–2092.
[17] I. Suorsa, E. Pagounis, K. Ullakko, Applied Physics Letters 84 (2004) 4658.
[18] C.H Yu, W.H. Wang, J.L. Chen, G.H. Wu, F.M. Yang, N. Tang, S.R. Qi, W.S. Zhan, Journal of Applied Physics 87 (2000) 6292–6294.
[19] A.A. Likhachev, A. Sozinov, K. Ullakko, Mechanics of Materials 38 (2006) 551–563.
[20] C. Seguí, E. Cesari, J. Pons, V. Chernenko, Materials Science and Engineering A 370 (2004) 481–484.